International Journal for Multidisciplinary Research (IJFMR)
E-ISSN: 2582-2160 ● Website: www.ijfmr.com ● Email: editor@ijfmr.com

High Field Confinement Enhancement in Silicon-based Photonic Crystal with Different Point Defects

Ferdousi Mayoa[1], Mehedi Hasan[2]

[1]Lecturer, Department of EEE, Noakhali Science and Technology University
[2]Student, Department of EEE, Bangladesh University of Engineering and Technology

Abstract

Two-dimensional silicon-based photonic crystals as optical analogs to electronic semiconductors are presented in this paper, emphasizing the design and analysis of two-dimensional structures. Employing the Lumerical FDTD solver, we initially crafted defect-free photonic crystals within a hexagonal lattice of air holes on a silicon slab (6.57 μm along x, 6.57 μm along y, 0.75 μm along z). The lattice parameters (a = 0.365 μm, r = 0.1095 μm, with r = 0.3a) established a target resonant wavelength of 1.5 μm. Utilizing Finite Difference Time-Domain (FDTD), we evaluated electric field decay, resonant modes, and the Q factor. The defect-free structure exhibited a peak Q factor of 736.004 at a resonant wavelength of 1262.87 nm. Removal of a central hole enhanced the Q factor to 1286.96 at 1391.07 nm. Introducing various line defects, the structure with three holes removed from vertical positions emerged as the optimal candidate for silicon-based photonic crystal cavity resonators, displaying the highest Q factor near the target resonant wavelength. Additionally, the structure with seven holes removed showed stable linear decays at both resonant wavelengths, suggesting its potential as a cavity resonator design candidate.

Keywords: Photonic Crystal, Silicon Slab, Crystal Defect, FDTD, Field Confinement

1. Introduction

Silicon, renowned for its elevated dielectric constant (ε(r)), is the prevailing material in modern microelectronics. Its remarkable dielectric contrast with air establishes Silicon as a compelling choice for investigating photonic crystal studies[1-5]. The discussed photonic crystal in this paper exhibits periodicity in the xy-plane and translational invariance along the z-axis, leading to the separation of modes into TE (transverse electric) and TM (transverse magnetic) polarizations. A complete photonic band gap, applicable to all directions and polarizations, is achieved at normalized frequencies $\omega_a/2\pi c$[6]. The TE photonic bandgap is notably wider than its TM counterpart[7], influencing the overall bandgap width. Customizing these parameters provides opportunities for tailored optical properties, opening avenues for fundamental research and applications in optoelectronics and photonics. Photonic crystal cavities, crucial in diverse applications[8-11], are introduced by forming a point defect—typically a single omitted hole—in a perfectly periodic photonic crystal slab. This defect breaks translational symmetry[12], allowing the emergence of localized modes within the photonic band gap. The lateral confinement of energy in these modes, due to the absence of propagating modes within the bandgap, is explored alongside the continuous k-vector spectrum of spatially localized modes. Vertically coupling these cavities by illuminating from

the top is common in practice, as in-line coupling concepts can distort symmetry and cause resonance splitting.

A line defect cavity[13, 14], an extension of the point defect concept, spans multiple lattice constants. Despite lower-than-expected Q-factors compared to point defects, strategic modifications, like shifting holes at defect edges, enhance Q-factors up to 45,000. Supporting standing wave-like modes with exponential field decay, these cavities can be vertically or side-coupled. Side-coupled variants function as compact Wavelength Division Multiplexing (WDM) channel drop filters, offering selective channel filtration while transmitting others [15]. Double heterostructure cavities [16, 17], composed of three photonic crystal line defect waveguides with different lattice constants, achieve the highest reported Q-factors. By omitting a row in the bulk photonic crystal, a line defect waveguide forms, confining guided modes within the bandgap. The resulting cavities exhibit high Q-factors (2.5 x 10^6) with small mode volumes, resembling Fabry-Perot resonators. They can be transmission-coupled, showing a sharp peak at resonance within a near-zero transmission frequency interval. This design holds potential for applications like integrated Wavelength Division Multiplexing (WDM) channel select filters or compact electro-optic modulators.

Our focal point in this analysis revolves around a Silicon-based photonic crystal structure—a Silicon slab intricately designed with a triangular lattice of holes, enveloped by air. The adoption of a triangular lattice imparts a notably broader Bandgap, introducing enhanced symmetry and a smoother Brillouin Zone.

2. Theory and Simulation Results

The inception of photonic crystals resulted from combining a quantum mechanical interpretation of Maxwell's equation with the application of the Bloch-Floquet theorem [18]. This led to the development of the Master equation [19] for photonic crystals, which integrates Maxwell's equations, source-free Faraday's law, and Ampere's laws at a specific frequency.

$$\overrightarrow{(\nabla} \times i\vec{\mathrm{k}}) \times \frac{1}{\varepsilon}\overrightarrow{(\nabla} \times i\vec{\mathrm{k}}) \times \vec{H}_{n,\vec{\mathrm{k}}} = (\frac{\omega_n(\vec{\mathrm{k}})}{\mathrm{C}})^2 \vec{H}_{n,\vec{\mathrm{k}}} \qquad (1)$$

The equation, featuring the dielectric function (ε) and the speed of light (c), imposes constraints on the energy and frequency of photons in crystals with regularly changing dielectric constants, creating a bandgap where no photons can exist [20]. The Master equation is crucial for identifying and analyzing eigenmodes in various photonic structures, including the study of confined eigenmodes in cavity resonators and defect modes introduced by anomalies in the cavity. Numerical methods, such as the Finite-difference time-domain (FDTD) method, are employed for analysis, with software like Lumerical FDTD solutions utilizing finite-difference approximations to explore photonic bandgap structures in detail.

The Q factor, or quality factor, in the context of photonic cavities, quantifies the rate of decay of the confined field within the cavity. In Lumerical FDTD Solutions Q factor is:

$$Q = \frac{-\omega_r \log_{10}(e)}{2m} \qquad (2)$$

where, ω_r is the resonant frequency and m is the slope of the log of the time signal. A higher Q-factor implies slower oscillation decay and lower energy loss in the resonator. The Q-factor is crucial for describing decay processes and is inversely proportional to energy loss. Total Q-factor is defined by [21]:

$$\frac{1}{Q_{total}} = \frac{1}{Q_{vertical}} + \frac{1}{Q_{horizontal}} \qquad (3)$$

Horizontal Q-factor can be controlled by adjusting the adjacent photonic crystal bulk size, while vertical Q-factor optimization is less significant. Mode delocalization, achieved by enlarging the cavity mode volume, reduces energy within leaky k-vector components [22]. However, a larger mode volume is

undesirable for device miniaturization and maintaining high optical field strength in nonlinear applications. To minimize k-vector components within the light cone, an alternative method involves aligning the symmetry of the Fourier transform of the cavity mode [23], preventing radiation into free space. In tentative scenarios, coupling light through a strip waveguide on the same substrate introduces an additional loss mechanism, reducing the horizontal Q-factor [24]. The vertical Q-factor is interconnected with the horizontal Q-factor and maximal transmission T_{max} through the relation

$$T_{max} = \left(\frac{Q_{total}}{Q_{horizontal}}\right)^2 = \left(\frac{Q_{vertical}}{Q_{vertical}+Q_{horizontal}}\right)^2 \quad (4)$$

Achieving close-to-unity transmission requires significantly larger leakage through coupling than through vertical radiation, with high transmission possible only when the horizontal Q-factor is much smaller than the vertical Q-factor.

In our study of Photonic Crystals, we examined a hexagonal Silicon-based array with periodicity along the x and y directions, and homogeneity along the z direction. The Silicon Slab dimensions are 6.57 μm, 6.57 μm, and 0.75 μm along x, y, and z, respectively. An array of air holes with a lattice constant (a) of 0.365 μm and hole radius (r) of 0.1095 μm was introduced. The array consists of 11 rows and 11 columns of air holes. The target resonant wavelength is set to 1.5 μm, with Silicon refractive index (n) at 3.45. Two electric dipole sources spanning wavelengths from 1.3 μm to 1.7 μm are placed for illumination. Resonant modes, structure variations, and Q factors at respective resonant wavelengths were observed [18, 19, 25]. Mode profiles for magnetic field components were examined at these resonant frequencies. Simulations were performed using the Lumerical FDTD solver software.

Hexagonal Photonic Crystal array without defect

Figure 1: (a) Refractive index profile where maroon indicates silver with RI=3.45 and blue indicates air with RI=1, (b) Magnetic field intensity with respect to position in the XY-plane, (c) Decay of the electric field components E_x, E_y and E_z and their respective envelopes, (d) The three intense modes have been identified using Gaussian filters, (e) the normalized intensities of the two most intense modes, (f) Rate of decay of the electric field at the two resonant modes

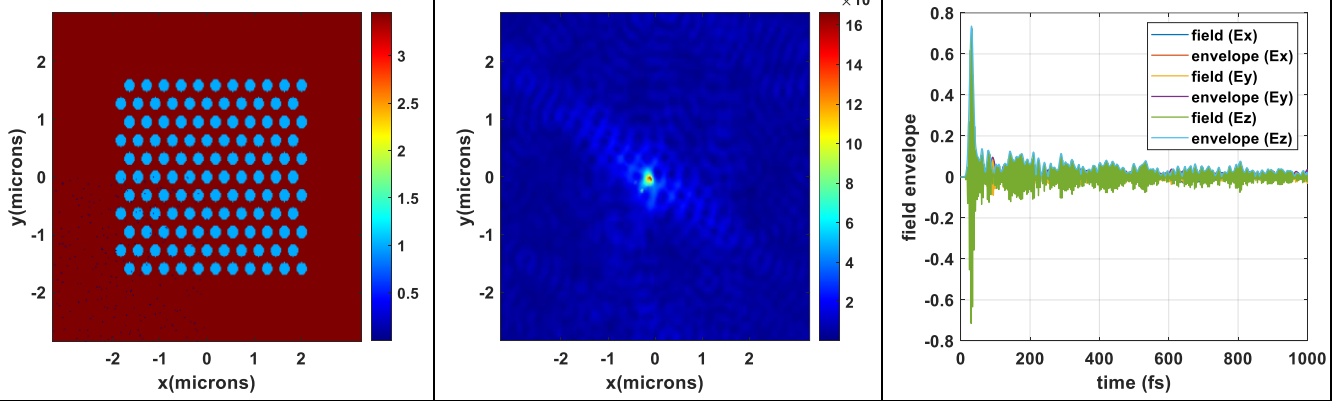

(a) (b) (c)

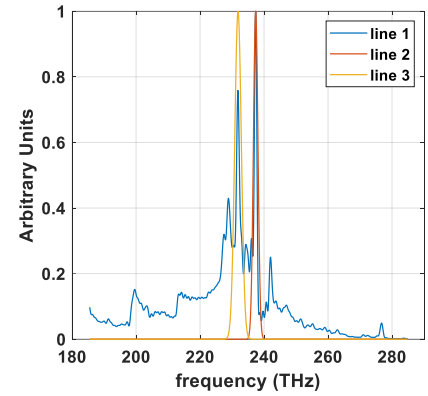

(d)

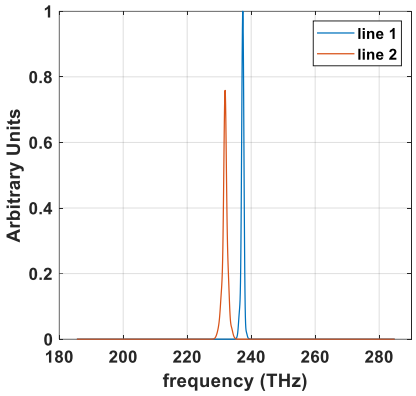

(e)

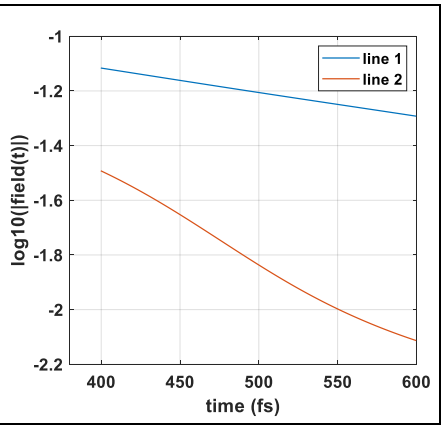

(f)

Initially, we examined a defect-free Silicon-based hexagonal photonic crystal, representing the refractive index profile in Figure 1(a). Magnetic field intensity H with respect to position in the xy-plane is illustrated in Figure 1(b). Air hole radius (r) is set as 0.3a, with a lattice constant a=0.365 μm at the target wavelength of 1.5 μm. Illuminating the structure with a dipole source yielded decay components of electric fields in x, y, and z-directions, as shown in Figure 1(c)[19]. Figure 1(c) illustrates the fast decay of electric field components inside the photonic crystal, indicating field confinement. The dipole source orientation at 0 degrees corresponds to Transverse Magnetic (TM) incident waves, leading to faster decay of Ex and Ey compared to Ez.

Normalized intensity comparison for the entire wavelength range and the three most intense TM modes is depicted in Figure 1(d). A Gaussian filter distinguishes these modes (Figure 1(e)), revealing resonant modes at 1262.87 nm and 1292.93 nm, or frequencies of 237.39 THz and 231.87 THz, respectively. The highest intensity occurs at 231.87 THz or 1292.93 nm due to the photonic crystal's dimensions and high refractive index contrast between Silicon slab and air holes. Figure 1(f) displays the rates of decay of electric fields at these resonant frequencies, with flatter curves indicating slower decay and better mode confinement, while steeper slopes suggest poorer confinement. The calculated Q factors for these modes at the resonant frequencies are shown in Table 4.1.

Hexagonal Photonic Crystal array with a point defect

Figure 2: (a) Refractive index profile where maroon indicates silver with RI=3.45 and blue indicates air with RI=1, (b) Magnetic field intensity with respect to position in the XY-plane, (c) Decay of the electric field components E_x, E_y and E_z and their respective envelopes, (d) The three intense modes have been identified using Gaussian filters, (e) the normalized intensities of the two most intense modes, (f) Rate of decay of the electric field at the two resonant modes

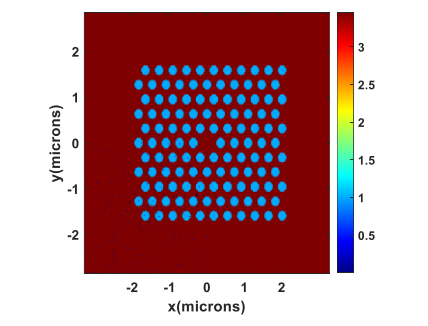

(a)

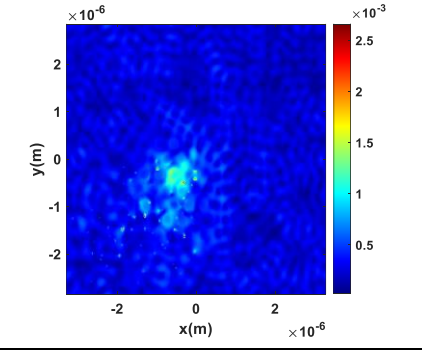

(b)

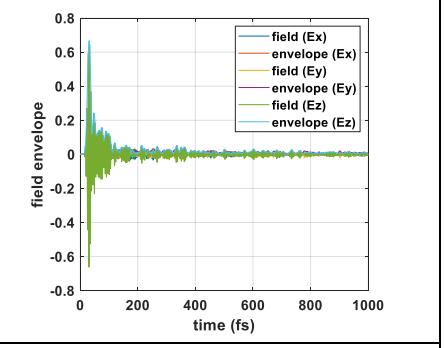

(c)

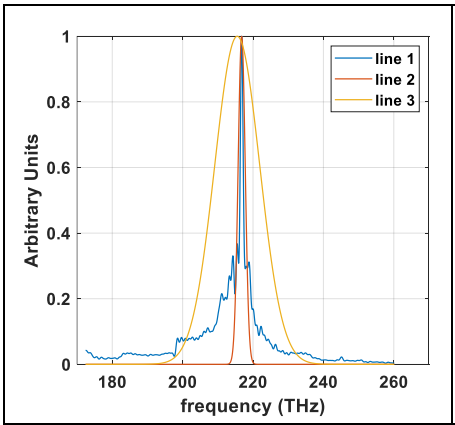

(d)

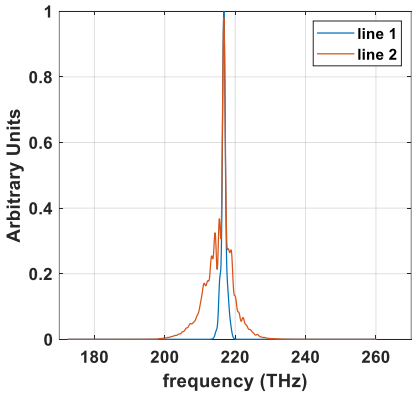

(e)

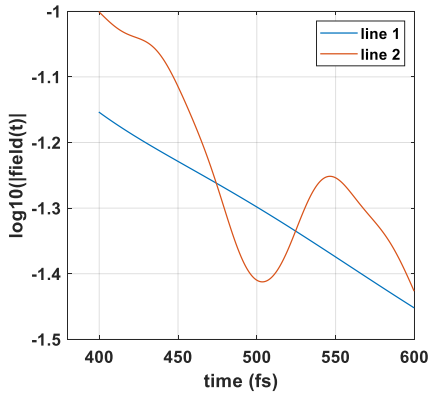

(f)

We introduced a point defect by removing the central air hole in the crystal, disrupting translational symmetry, as shown in Figure 2 (a). This alteration results in a single localized mode or closely spaced modes within the photonic band gap. The decay of the electric field components is faster compared to the structure without defects, indicating improved magnetic field confinement (Figure 2 (c)).

Normalized intensity for the frequency range is depicted in Figure 2 (d), and the two most intense modes are highlighted in Figure 2 (e). The maximum intensities occur at wavelengths of 1382.96 nm and 1391.07 nm, with the latter having the highest intensity. Figure 2 (f) illustrates the rate of decay of the magnetic field at these wavelengths. Q factors, calculated from the decay rates, are listed in Table 1. The highest Q factor, 1286.96, corresponds to the resonant mode at 1391.07 nm. Contour plots of the simulated magnetic field intensity along the xy-plane are presented in Figure 2 (b), emphasizing concentrated magnetic fields at the defect. Introducing a point defect significantly improves the Q factor and field confinement.

Hexagonal Photonic Crystal array with line defect

We introduced a line defect by removing five consecutive air holes in the photonic crystal. Figure 3 (a) shows the refractive indices at different spatial positions, and Figure 3 (c) illustrates the decay of electric field components in X, Y, and Z directions over time. The slower decay in the z-direction indicates TM modes.

Figure 3: (a) Refractive index profile where maroon indicates silver with RI=3.45 and blue indicates air with RI=1, (b) Magnetic field intensity with respect to position in the XY-plane, (c) Decay of the electric field components E_x, E_y and E_z and their respective envelopes, (d) The three intense modes have been identified using Gaussian filters, (e) the normalized intensities of the two most intense modes, (f) Rate of decay of the electric field at the two resonant modes

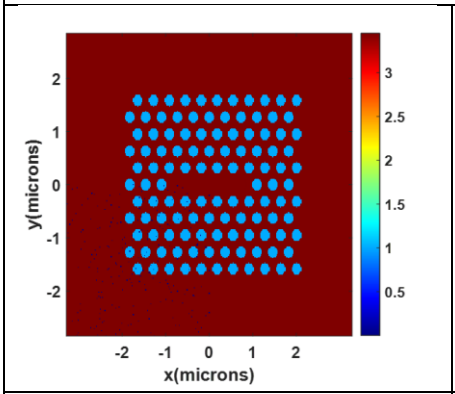

(a)

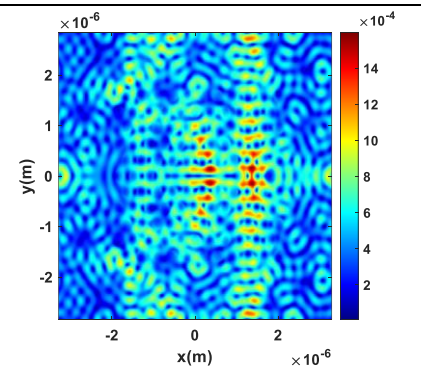

(b)

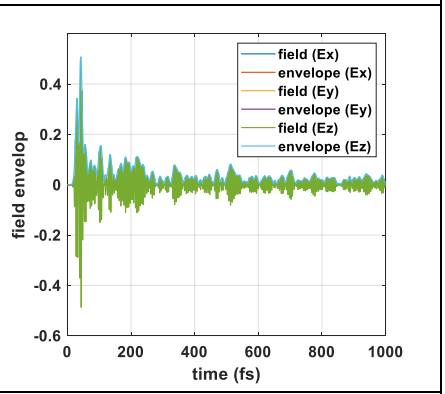

(c)

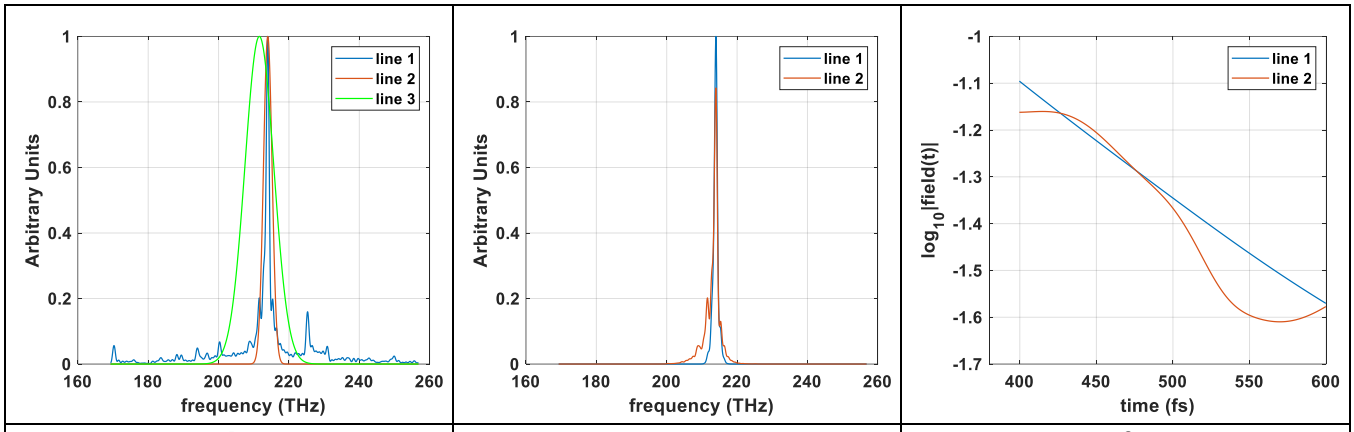

(d) (e) (f)

Normalized intensity comparison for the entire wavelength range is in Figure 3 (d), with the two most intense modes highlighted in Figure 3 (e). These modes occur at wavelengths of 1397.54 nm and 1389.35 nm. Figure 3 (f) depicts the rate of decay of the electric field over time. Q factors were calculated at the resonant wavelengths, with higher values for 1397.54 nm. The slower decay of the magnetic field for 1397.54 nm is evident in Figure 3 (f). The simulated contour plot of the magnetic field intensity H is in Figure 3 (b), showing strong periodic confinement of light in the region of the line defect. However, the highest Q factor obtained for this structure is lower than that for the defect-free photonic crystal.

Hexagonal Photonic Crystal array with 3 holes removed

In the case of introducing a vertical line defect by removing three consecutive air holes, the refractive index profile concerning spatial positions is illustrated in Figure 4 (a). The decay of electric field components in X, Y, and Z directions over time for this structure is shown in Figure 4 (c). The electric field component along the z-direction decays comparatively slower, indicating TM modes.

Figure 4: (a) Refractive index profile where maroon indicates silver with RI=3.45 and blue indicates air with RI=1, (b) Magnetic field intensity with respect to position in the XY-plane, (c) Decay of the electric field components E_x, E_y and E_z and their respective envelopes, (d) The three intense modes have been identified using Gaussian filters, (e) the normalized intensities of the two most intense modes, (f) Rate of decay of the electric field at the two resonant modes

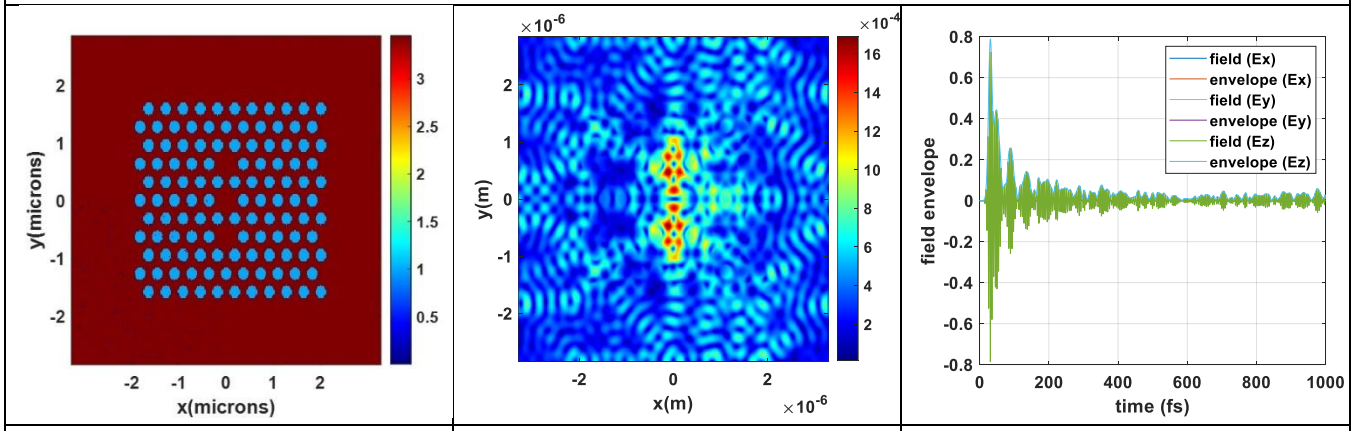

(a) (b) (c)

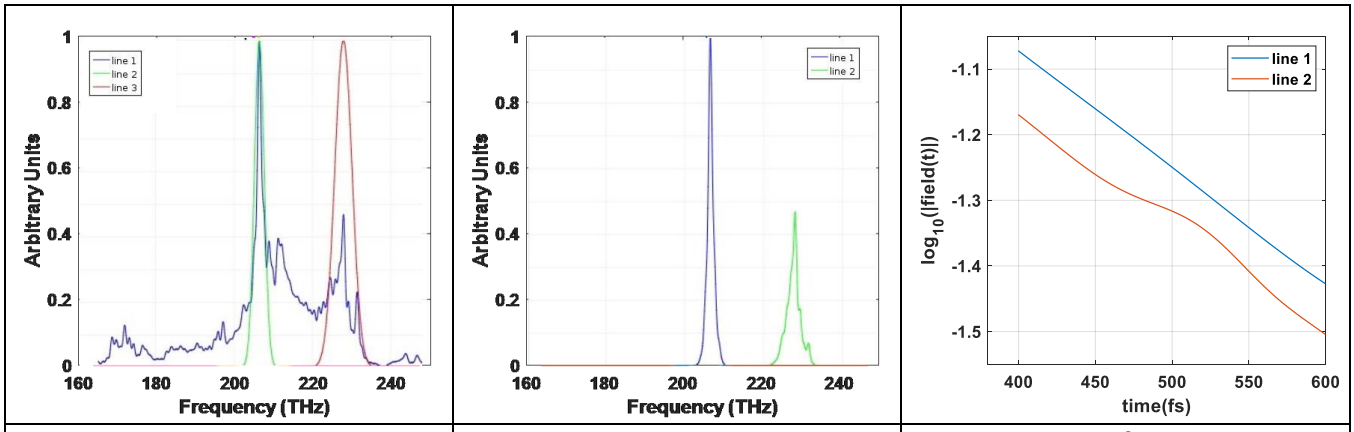

(d) (e) (f)

Figure 4 (d) presents the normalized intensity for the entire frequency range, and Figure 4 (e) displays the normalized intensities for the two most intense modes. The two maximum intensities occur at wavelengths of 1452.94 nm and 1315.7 nm, corresponding to frequencies of 206.336 THz and 227.857 THz. Figure 4 (f) illustrates the rate of decay of the electric field at these two wavelengths over time. The calculated Q factors, obtained from the slopes of the decay rates, are listed in Table 1. The FDTD simulated contour plot of magnetic field intensity concerning position is shown in Figure 4 (b).

Hexagonal Photonic Crystal array with 7 holes removed

In this case, six air holes were removed from the vertical positions relative to and along with the central air hole., and Figure 5 (a) shows refractive indices with respect to spatial positions. The decay of the three electric field components over time is presented in Figure 5 (c). Normalized intensity for the entire frequency range is compared in Figure 5 (d), and Figure 5 (e) shows the normalized intensities for the two most intense modes. The two maximum intensities occur at wavelengths of 1197.46 nm and 1190.51 nm, with corresponding frequencies of 250.356 THz and 251.819 THz (Figure 5 (e)). The rate of decay of the magnetic field at these wavelengths is depicted in Figure 5 (f). Q factors at these wavelengths are tabulated in Table 1. The FDTD simulated contour plot of the magnetic field intensity is shown in Figure 5(b) providing insights into mode confinement in the cavity formed by removing seven air holes.

Figure 5: (a) Refractive index profile where maroon indicates silver with RI=3.45 and blue indicates air with RI=1, (b) Magnetic field intensity with respect to position in the XY-plane, (c) Decay of the electric field components E_x, E_y and E_z and their respective envelopes, (d) The three intense modes have been identified using Gaussian filters, (e) the normalized intensities of the two most intense modes, (f) Rate of decay of the electric field at the two resonant modes

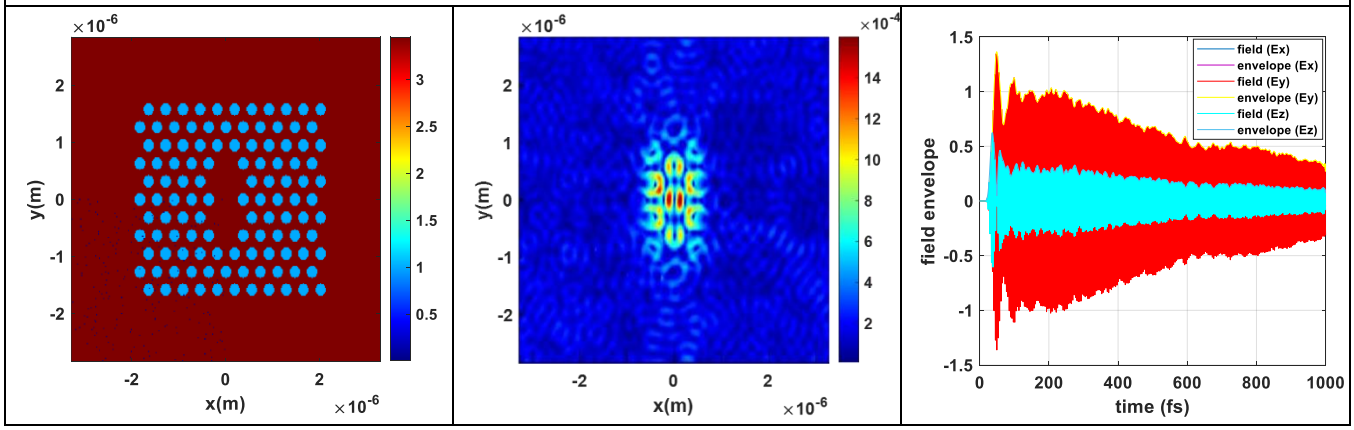

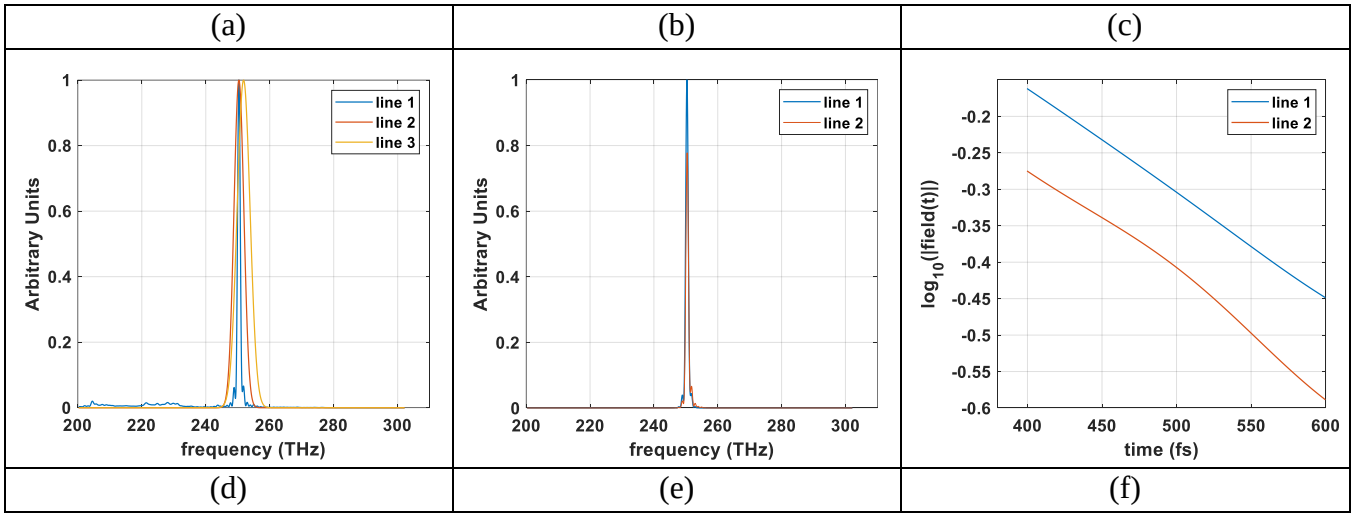

Table 1: Q factor at two modes of different structures

Structures	Resonant Modes	Wavelength (nm)	Frequency (THz)	Q factor
HPC without defect	Mode 1	1292.93	231.87	203.868 ± 35.3642
	Mode 2	1262.87	237. 39	736.004 ± 12.8247
HPC with a point defect	Mode 1	1391.07	215.513	1286.96 +/- 10333.6
	Mode 2	1382.96	216.776	305.462 +/- 45.5857
HPC with line defect	Mode 1	1397.54	214.515	217.275 +/- 11.1565
	Mode 2	1389.35	215.779	185.408 +/- 163.237
HPC with 3 holes removed	Mode 1	1452.94	206.336	201.142 +/- 23.0559
	Mode 2	1315.7	227.857	591.963 +/- 4074.3
HPC with 7 holes removed	Mode 1	1197.46	250.356	476.526 +/- 16.1707
	Mode 2	1190.51	251.819	438.103 +/- 75.2017

3. Conclusion

In the pursuit of optimizing field confinement within a silicon slab adorned with air holes, a meticulous design and simulation approach was employed to create five distinct photonic crystal cavity resonators. Through a systematic removal of air holes, a strategic configuration was sought to achieve superior field confinement, as indicated by elevated Q factors and frequency domain surface profiles. Among the various structures explored, the hexagonal photonic crystal resonator, characterized by the removal of seven holes in a vertical arrangement, emerged as the most promising, exhibiting consistent and heightened field confinement.

4. Conflict of Interest

The authors declare no conflicts of interest.

5. References

1. Chen, X., et al., “Efficient Frequency Upconversion Photodetection in Heterojunction of InSe and Silicon Photonic Crystal Cavity”. Advanced Optical Materials: p. 2301468.
2. Lezhennikova, K., et al., “Terahertz near-field suppression and multiplexing with a silicon photonic crystal”. arXiv:2310.01715, 2023.

3. Anandan, S., et al., "A low loss hexagonal six-port optical circulator using silicon photonic crystal". Optical and Quantum Electronics, 2023. **55**(12): p. 1092.
4. Liu, L., et al., "Silicon photonic crystal ring resonator with high-quality-factor". IEEE Photonics Technology Letters, 2023.
5. Avi, S. and S. Bhattacharya. "Silicon Photonic Crystal Architecture for Ultra-Thin, High-Efficiency Single Photon Detectors". in 2023 Photonics & Electromagnetics Research Symposium (PIERS). 2023. IEEE.
6. Chau, Y.-F., et al., "Evolution of the complete photonic bandgap of two-dimensional photonic crystal". Optics express, 2011. **19**(6): p. 4862-4867.
7. Liu, X.-J., et al., "Two-dimensional function photonic crystals". Physica E: Low-Dimensional Systems and Nanostructures, 2017. **85**: p. 227-237.
8. Li, C., et al., "MoTe2 PN homojunction constructed on a silicon photonic crystal cavity for high-performance photodetector". ACS Photonics, 2021. **8**(8): p. 2431-2439.
9. Watanabe, K., et al., "Single virus detection on silicon photonic crystal random cavities". Small, 2022. **18**(15): p. 2107597.
10. Mauthe, S., et al., "Hybrid III–V silicon photonic crystal cavity emitting at telecom wavelengths". Nano Letters, 2020. **20**(12): p. 8768-8772.
11. Chen, X., et al., "Multifunctional optoelectronic device based on graphene-coupled silicon photonic crystal cavities". Optics Express, 2021. **29**(7): p. 11094-11105.
12. Bayindir, M., et al., "Photonic band gaps, defect characteristics, and waveguiding in two-dimensional disordered dielectric and metallic photonic crystals". Physical Review B, 2001. **64**(19): p. 195113.
13. Baba, T., et al., "Light localizations in photonic crystal line defect waveguides. IEEE Journal of selected topics in quantum electronics", 2004. **10**(3): p. 484-491.
14. Asano, T. and S. Noda, "Photonic crystal devices in silicon photonics". Proceedings of the IEEE, 2018. **106**(12): p. 2183-2195.
15. Akahane, Y., et al., "Investigation of high-Q channel drop filters using donor-type defects in two-dimensional photonic crystal slabs". Applied Physics Letters, 2003. **83**(8): p. 1512-1514.
16. Wang, L.-F., et al., "Mode selection in InGaAs/InGaAsP quantum well photonic crystal lasers based on coupled double-heterostructure cavities". Optics Express, 2022. **30**(7): p. 10229-10238.
17. Kazanskiy, N.L., M.A. Butt, and S.N. Khonina. "2D-Heterostructure photonic crystal formation for on-chip polarization division multiplexing. in Photonics". 2021. MDPI.
18. Johnson, S.G. and J.D. Joannopoulos, "Introduction to photonic crystals: Bloch's theorem, band diagrams, and gaps (but no defects) ". Photonic Crystal Tutorial, 2003: p. 1-16.
19. Andreani, L.C. and M. Agio, "Photonic bands and gap maps in a photonic crystal slab". IEEE Journal of Quantum Electronics, 2002. **38**(7): p. 891-898.
20. Lourtioz, J.-M., et al., "Photonic crystals. Towards Nanoscale Photonic Devices", 2005.
21. Tanaka, Y., et al., "Dynamic control of the Q factor in a photonic crystal nanocavity". Nature materials, 2007. **6**(11): p. 862-865.
22. Johnson, S.G., et al., "Multipole-cancellation mechanism for high-Q cavities in the absence of a complete photonic band gap". Applied Physics Letters, 2001. **78**(22): p. 3388-3390.
23. Srinivasan, K. and O. Painter, "Momentum space design of high-Q photonic crystal optical cavities". Optics Express, 2002. **10**(15): p. 670-684.

24. Kim, G.-H., et al., “Coupling of small, low-loss hexapole mode with photonic crystal slab waveguide mode”. Optics Express, 2004. **12**(26): p. 6624-6631.
25. Krauss, T.F., R.M.D.L. Rue, and S. Brand, “Two-dimensional photonic-bandgap structures operating at near-infrared wavelengths”. Nature, 1996. **383**(6602): p. 699-702.